Inorganic Chemistry
Cite This: Inorg. Chem. XXXX, XXX, XXX−XXX
Article
pubs.acs.org/IC

Addressing Reversibility of R−NHC Coupling on Palladium: Is Nano-to-Molecular Transition Possible for the Pd/NHC System?

Ekaterina A. Denisova, Dmitry B. Eremin, Evgeniy G. Gordeev, Andrey M. Tsedilin, and Valentine P. Ananikov*

Zelinsky Institute of Organic Chemistry, Russian Academy of Sciences, Leninsky Prospect 47, Moscow 119991, Russia

Supporting Information

ABSTRACT: It has recently been shown that palladium-catalyzed reactions with N-heterocyclic carbene (NHC) ligands involve R−NHC coupling accompanied by transformation of the molecular catalytic system into the nanoscale catalytic system. An important question appeared in this regard is whether such a change in the catalytic system is irreversible. More specifically, is the reverse nano-to-molecular transformation possible? In view of the paramount significance of this question to the area of catalyst design, we studied the capability of 2-substituted azolium salts to undergo the breakage of C−C bond and exchange substituents on the carbene carbon with corresponding aryl halides in the presence of Pd nanoparticles. The study provides important experimental evidence of possibility of the reversible R−NHC coupling. The observed behavior indicates that the nanosized metal species are capable of reverse transition to molecular species. Such an option, known for phosphine ligands, was previously unexplored for NHC ligands. The present study for the first time demonstrates bidirectional dynamic transitions between the molecular and nanostructured states in Pd/NHC systems. As a unique feature, surprisingly small activation barriers (<18 kcal/mol) and noticeable thermodynamic driving force (−5 to −7 kcal/mol) were calculated for C−C bond oxidative addition to Pd(0) centers in the studied system. The first example of NHC-mediated Pd leaching from metal nanoparticles to solution was observed and formation of Pd/NHC complex in solution was detected by ESI-MS.

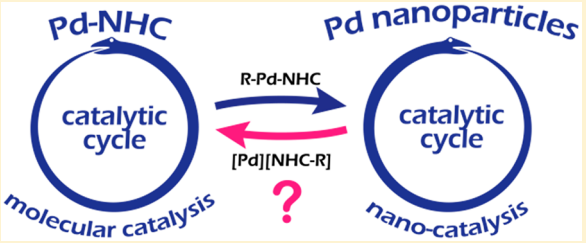

INTRODUCTION

N-heterocyclic carbenes (NHCs) are efficient ligands in homogeneous transition-metal catalysis. They gained world-wide recognition due to the impressive variety of compounds of this type and the wide range of their applications.[1] As ligands, NHCs are indispensable for cross-coupling, C−H functionalization, Mizoroki−Heck reaction, metathesis and carbon−heteroatom bond formation,[1,2] synthesis of biologically active molecules, and advanced materials development.[3]

The high stability of metal/NHC (M/NHC) complexes is conventionally explained by electron-donating properties of NHC rings enhanced by steric hindrance conferred by substituents on nitrogen atoms.[1,2,4] However, recent studies indicate that the remarkable catalytic activity of M/NHC complexes not only due is to their stability but also is largely dependent on the lability of the M−NHC bond under certain conditions.[5,6]

In particular, it has been shown that oxidative addition of organic halide to a metal complex proceeds rather easily and acts as a beginning stage for the subsequent R−NHC coupling.[7] The resulting NHC-free molecular palladium complex is prone to agglomeration causing transition of the molecular catalytic system into nanostructured state (arrow A in Scheme 1). This transition is manifested by formation of palladium nanoclusters and nanoparticles (NPs) which may act as a nanosized catalyst. Formation of metal NPs has been confirmed for a variety of M/NHC systems.[6] From the mechanistic point of view it is uncertain whether this transition is unidirectional or it can be reversed to switch the state back from nanostructured to molecular. If R−NHC coupling is irreversible under catalytic conditions, then the nanosized system (right part of Scheme 1) should be considered as the final stage of catalyst evolution in this case. Reversibility of R−NHC coupling would allow one to adjust the mode of catalysis (molecular vs nano) depending on the requirements of a specific task. This question is of key importance because completely different principles of catalyst design should be utilized for nanoscale and molecular systems. Indeed, doing rational catalyst design is hardly possible (or is totally impossible) without knowledge about catalytically active centers and without understanding possible pathways of dynamic interconversions of catalytic species.

Many reports describe the molecular-to-nanoscale conversion where R−NHC coupling generates Pd centers susceptible to agglomeration (arrow A in Scheme 1).[6a,b,7,8] Azolium salts produced by R−NHC coupling act as efficient stabilizers of NPs/colloidal systems.[1e,6a,9] In a series of excellent recent studies, Bullock and co-workers have shown

Received: June 3, 2019

DOI: 10.1021/acs.inorgchem.9b01630
Inorg. Chem. XXXX, XXX, XXX−XXX

Scheme 1. Direct Molecular-to-Nanoparticle and Reverse Nanoparticle-to-Molecular Transitions of Active Species in M/NHC Catalysis

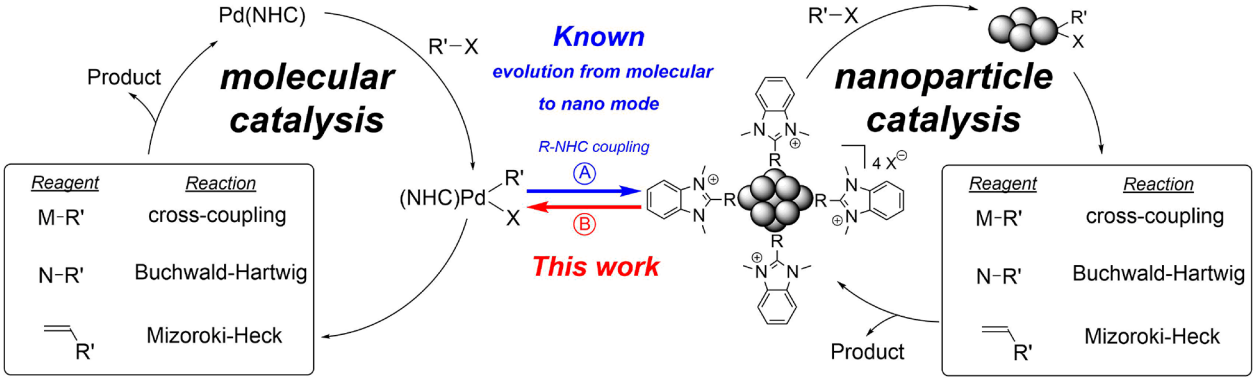

that Rh NPs stabilized by cyclic alkyl amino carbene (CAAC) ligands can behave as active species in arene hydrogenation. This hypothesis has been confirmed by a number of experimental methods, including kinetic studies, mechanistic studies involving a filtration test, fractional poisoning experiments, XAFS measurements, STEM characterization, and infrared spectroscopy. It was proposed that the presence of CAAC at the surface of catalytically active particles ensures their high reactivity.[9]

In contrast, no direct nanoscale-to-molecular transitions involving R−NHC$^+$X$^-$ compounds (arrow B in Scheme 1) has been described previously. The reverse process can be considered in terms of C−C bond activation and leaching. The effect of leaching is substantive when using phosphine complexes of Pd,[8] especially in the presence of organic halides, in order to facilitate formation of R−Pd−X species and removal of Pd atoms from the surface of nanoparticles.[10a] Mechanistic changes, metal contamination, and sustainability issues are important factors to be considered in the case of leaching.[10b,c]

Thus, the possibility of reversible R−NHC coupling can be associated with a particular type of leaching accompanied by the metal-mediated C−C bond breakage (arrow B in Scheme 1). This hypothetical process, with proper refinements, may be extremely useful in designing M/NHC catalytic systems, but from general considerations (high activation energies of C−C bond oxidative addition) this process cannot be regarded as very likely. In this experimental study, C−C bond breakage in the R−NHC coupling products is closely examined for the first time and unique feature of this transformation is revealed.

RESULTS AND DISCUSSION

Experimental examination of C−C bond breakage in the R−NHC coupling product was carried out in accordance with Scheme 2. In DMF, palladium acetate undergoes chemical reduction leading to formation of metal clusters and nanoparticles. Upon the addition of azolium salt R−NHC$^+$X$^-$ to the system, the metal particles are stabilized against agglomeration and precipitation. We propose that NHC-capped Pd NPs become capable of transformation into molecular palladium complex R−Pd−NHC after C−C bond breakage. This complex can be trapped by reaction with organic halides R′-X leading to formation of a different product. It is worth noting that the resulting azolium salt R′−NHC$^+$X$^-$ can also act as a stabilizer for Pd NPs. Indeed, without breakage of C-C bond in the starting azolium salt R−NHC$^+$X$^-$ formation of the R′−

Scheme 2. Reaction Scheme Used for Studying C−C Bond Breakage in the R−NHC/Pd System

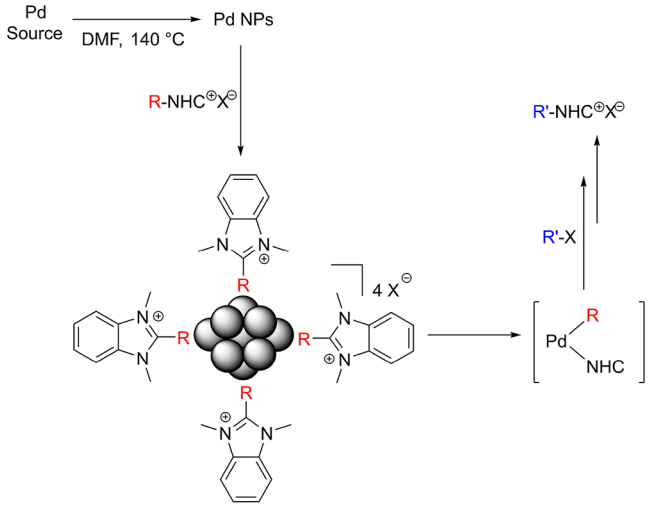

NHC$^+$X$^-$ reaction product (a different azolium salt) would be impossible. Its formation, therefore, suggests the possibility of R−NHC bond breakage by Pd clusters (Scheme 2). Being the key step toward the nano-to-molecular transformation of the studied system under catalytic conditions, this reaction models the process reverse to R−NHC coupling (Scheme 1B).

Observation of Palladium Nanoparticles. Formation of palladium nanoparticles (Pd NPs) from palladium acetate in DMF has been described previously.[11] We performed this process in order to characterize Pd NPs in DMF before using them in the experiment (Figure 1). The samples were prepared by heating of $Pd(OAc)_2$ solution in DMF for 1 h at 140°C. Concerning the temperature range, formation of Pd nanoparticles can be also observed at lower temperatures (75−100 °C; Supporting Information, Figure S24). According to the transmission electron microscopy (TEM) images, Pd NPs are formed efficiently under these conditions. Higher magnifications images (Figure 1, parts c and d) allow to distinguish overlaps of the atomic layers in palladium nanoparticles.

Computational Proof of Thermodynamic Driving Force of the Process. Quantum chemical modeling of the energy profile involving R−NHC coupling and the reverse process of R−NHC oxidative addition has been performed for the model system (Figure 2). Remarkably, the C−C bond in the starting complex **I** can be broken via overcoming of

DOI: 10.1021/acs.inorgchem.9b01630
Inorg. Chem. XXXX, XXX, XXX−XXX

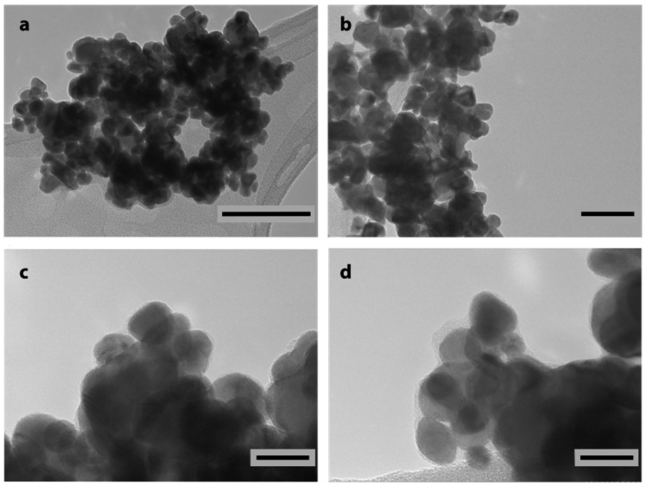

Figure 1. TEM images for Pd NPs forming from $Pd(OAc)_2$ in DMF at 140 °C. Scale bars: 100 nm (a), 50 μm (b); 20 μm (c and d).

relatively small energy barrier of $\Delta E^{\ddagger}_{I\rightarrow II\text{-}TS}$ = 9.9 kcal/mol ($\Delta G^{\ddagger}_{I\rightarrow II\text{-}TS}$ = 8.5 kcal/mol; NHC = BIMe).

The lowest activation energy of the Me-NHC oxidative addition is observed for NHC = IMe, whereas the highest activation energy ($\Delta E^{\ddagger}$ = 11.4; $\Delta G^{\ddagger}$ = 11.2 kcal/mol) is inherent in the process with the IPr as the NHC ligand. However, the differences in potential barriers of the methyl group transfer are small ($\Delta\Delta E^{\ddagger}$ = 3.5 kcal/mol), since the methyl group is characterized by a small spatial volume and, apparently, relatively weak interacts with NHC ligands of even a large volume. The reaction for complexes with all NHC ligands is thermodynamically favored, for example with the energy difference of $\Delta E_{I\rightarrow III}$ = −9.1 to −16.7 kcal/mol ($\Delta G_{I\rightarrow III}$ = −10.6 to −15.4 kcal/mol). A further gain in energy occurs upon transition from complex **III** to complex **IV**, as a result of substitution of methyl group with phenyl group. It should be noted that the energy gain upon replacement of Me with Ph is almost the same for different NHC ligands: ΔE (kcal/mol) = −5.2 (BIMe), −5.5 (IPr), −5.6 (IMe), and −6.3 (IMes).

Subsequent Ph−NHC coupling leads to product **VI** via the transition state **V-TS**, with $\Delta E^{\ddagger}_{IV\rightarrow V\text{-}TS}$ = 18.0−23.1 kcal/mol ($\Delta G^{\ddagger}_{IV\rightarrow V\text{-}TS}$ = 17.9−22.1 kcal/mol) for the studied NHC ligands. However, it can be noted that the activation energy of the R−NHC coupling (**IV** → **V-TS** for the Ph−NHC coupling and **III** → **II-TS** for the Me−NHC coupling) increases in the following order IMes > IPr > IMe ∼ BIMe. This pattern may be related to the strength of the metal−ligand bond and the influence of steric hindrance.

The product **VI** is more stable than the starting complex **I** (ΔE = −9.3 to −15.0 kcal/mol; ΔG = −7.9 to −13.1 kcal/mol for the studied complexes). Thus, the replacement of alkyl substituent with phenyl substituent in the studied R−NHC/Pd system is thermodynamically favorable for all NHC ligands under consideration. It should be noted that activation energies of R−NHC coupling for different R are very similar, e.g. $\Delta E^{\ddagger}_{III\rightarrow II\text{-}TS}$ = 19.0−24.7 kcal/mol for R = Me and $\Delta E^{\ddagger}_{IV\rightarrow V\text{-}TS}$ = 18.0−23.1 kcal/mol for R′ = Ph ($\Delta G^{\ddagger}$ = 19.1−24.2 and 17.9−22.1 kcal/mol, respectively for the studied NHC systems).

Thus, the theoretical calculations reveal thermodynamic driving force for the alkyl/aryl substitution in the studied R−NHC system. The observed stabilization may be explained by a more efficient Pd−Ar interaction as compared with a Pd−Alk

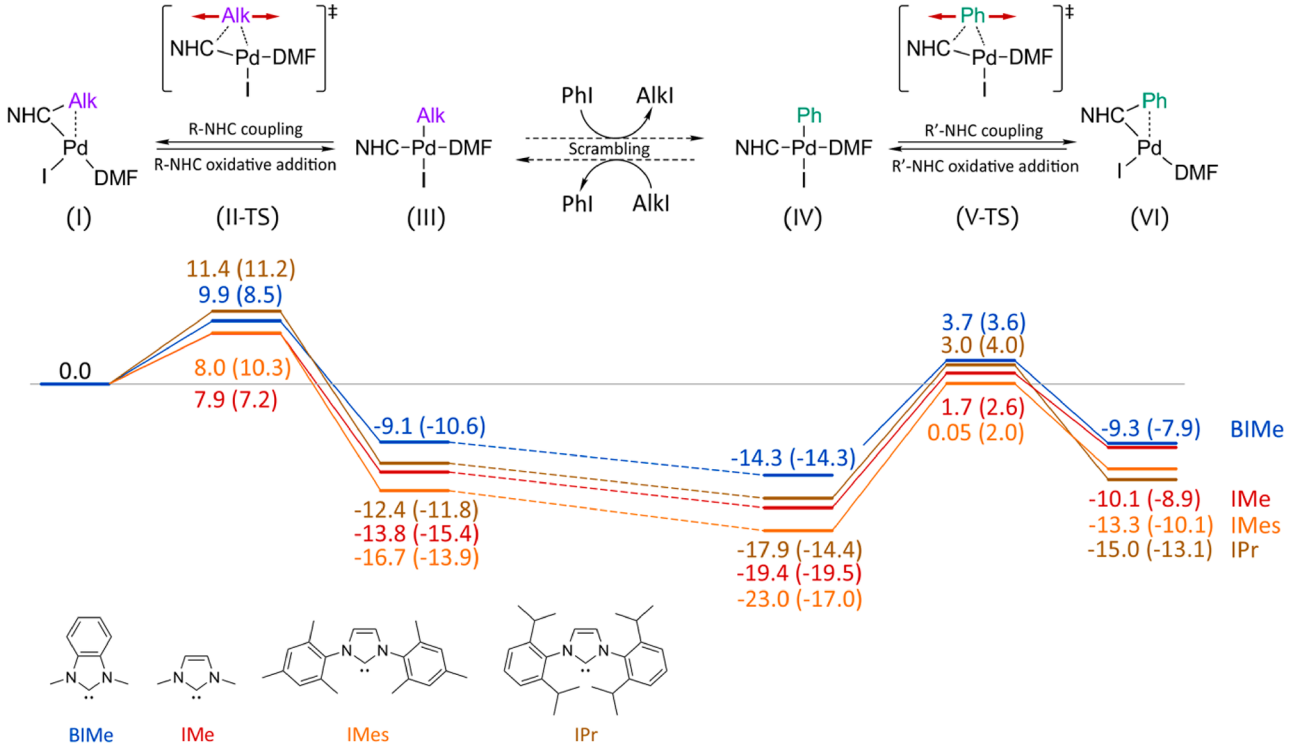

Figure 2. Calculated energy profile with total energies (ΔE, kcal/mol) and Gibbs energies (ΔG, kcal/mol, in parentheses) for each stage at the PBE1PBE/6-311G(d)&def2TZVP D3BJ level (Alk = Me; NHC = BIMe, IMe, IMes, IPr). Scrambling stage is shown formally to compare relative energies (mechanistic pathways are discussed in detail later).

DOI: 10.1021/acs.inorgchem.9b01630
Inorg. Chem. XXXX, XXX, XXX−XXX

interaction (**IV** vs **III**), as well as by contribution of a larger bond energy of Ar−NHC as compared to Alk-NHC (**VI** vs **I**).

It should be noted that in this section we only model the overall thermodynamic driving force. More detailed computational consideration of different reaction channels will be given in subsequent sections, and its relation to experimental findings will be thoroughly addressed.

Analytical Assessment of the R−NHC Transformation on Pd by Mass Spectrometry and Nuclear Magnetic Resonance. For experimental study, the corresponding system was chosen as a suitable model for studying the reaction of R−NHC with Pd by electrospray ionization high-resolution mass spectrometry (ESI-MS) and nuclear magnetic resonance spectroscopy (NMR) (Scheme 3). The interaction

Scheme 3. Model Reaction Used for Studying Interactions of R−NHC species with Pd by Mass Spectrometry and NMR Spectroscopy and Calculated Bond Energies

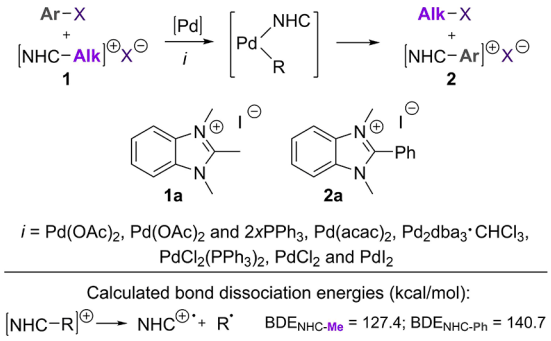

of Me-substituted starting material **1a** with iodobenzene was studied in the presence of equimolar amount of palladium from different sources. As a result of the studied reaction, Ph-substituted product **2a** was formed (Scheme 3). According to the theoretical calculations discussed above, the exchange process leading to substitution of methyl group with phenyl group should be energetically favored (Figure 2). Regarding the final products, the calculations have shown that the NHC−Ph bond is by 13.3 kcal/mol stronger as compared to the NHC-Me bond (Scheme 3). Formation of the target product, 1,3-dimethyl-2-phenyl-1*H*-benzimidazol-3-ium iodide (**2a**), was monitored by ESI-MS (Figure 3). Signal intensities for molecular cations of azolium salts **1a** and **2a** (m/z 161 and 223 respectively) were measured at the moment the reaction was launched and after 24 h.

At the beginning of the reaction, no traces of the product were detected for all of the experiments, which excluded the possibility of in-source formation of **2a**. The maximal intensity of signal for molecular ion **2a** was achieved in the reaction with $Pd(OAc)_2$. It should be noted that the use of triethylamine as a base suppressed formation of the m/z 223 molecular ion in all cases. The possibility of this reaction to take place with other metals was also tested under similar conditions. The reaction proceeded well in the presence of copper salts, with lower reactivity in the presence of nickel salts and did not proceed in the presence of cobalt salts (Supporting Information, Table S4).

Quantitative identification of the reaction product formation was carried out by NMR for the three most efficient systems selected on the basis of the results of mass spectrometry: $Pd(OAc)_2$, $Pd(OAc)_2/PPh_3$, and $Pd(acac)_2$. In all three cases, the ^{1}H NMR spectra recorded after 24 h contained new signal

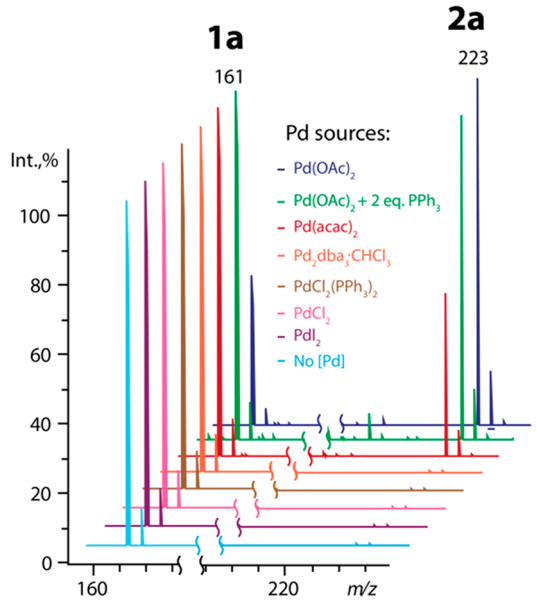

Figure 3. Normalized mass spectra of the reaction mixtures with different Pd sources after 24 h (0.1 mmol **1a**, 0.2 mmol PhI, 1 equiv of [Pd], DMF, 140 °C).

in the upfield region at δ 3.89 ppm (Figure 4). This signal corresponds to the *N*-Me groups of Ph-substituted azolium salt

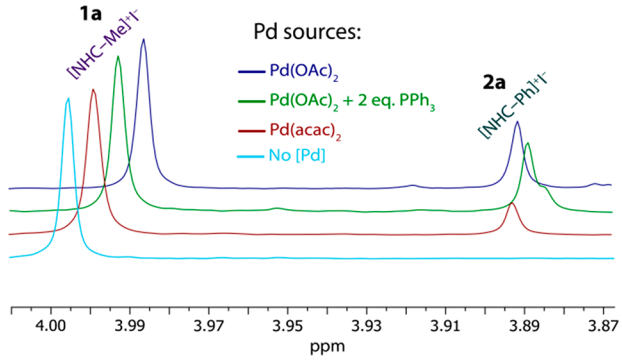

Figure 4. ^{1}H NMR spectra of the reaction mixtures with different Pd sources after 24 h (0.1 mmol **1a**, 0.2 mmol PhI, 1 equiv of [Pd], DMF, 140 °C).

2a. The control experiments confirmed participation of Pd in the reaction (no corresponding transformation was observed in the absence of Pd).

Kinetics of the R−NHC exchange was studied by ^{1}H NMR monitoring (Figure 5) using $Pd(OAc)_2$ as a source of palladium. Within 1 h after beginning of the reaction, at 25% conversion of the starting **1a**, the yield of **2a** was about 20%. After 24 h of the reaction, the product yield reached a plateau of 31%, whereas conversion of **1a** at this point was close to 44%, which suggests the presence of side reactions that also consume the azolium salt. Accordingly, toluene, iodomethane, and biphenyl (the product of iodobenzene homocoupling) were detected in the reaction mixture by GC-MS. The product **2a** was isolated from the mixture in 20% yield by flash chromatography. Kinetic curves, with built in $C = f(t)$, $\ln C = f(t)$, $1/C = f(t)$, and $1/C^2 = f(t)$ coordinates on the basis of experimental data, are nonlinear.

DOI: 10.1021/acs.inorgchem.9b01630
Inorg. Chem. XXXX, XXX, XXX−XXX

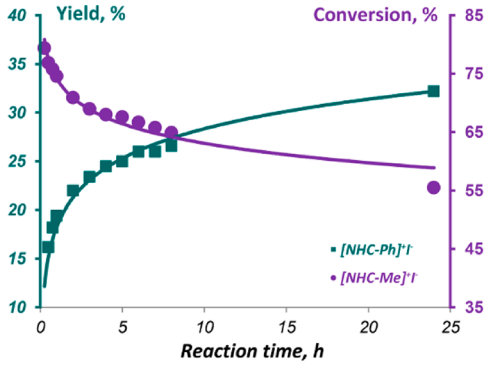

Figure 5. ^{1}H NMR monitoring of R,R′−NHC coupling (**1a**, PhI, 1 equiv of $Pd(OAc)_2$, DMF, 140 °C).

Thus, the computationally predicted possibility of substitution of the methyl group ($-CH_3$) at the carbon in the second position of benzimidazolium ring by phenyl group (−Ph) has been confirmed experimentally. It is evident therefore that the C−C bond in the R−NHC molecular framework can be broken in the presence of Pd nanoparticles.

Reversible R,R′−NHC Coupling under Various Conditions. Reversibility of R−NHC coupling was evaluated for a range of conditions (Table 1) and the following trends can be

Table 1. Proceeding of R−NHC Coupling Observed under Various Conditions

	variable parameter			
no.			ESI-MS[a] **2** signal[b]	^{1}H NMR yield of **2**[b] (%)
1	ArX	(*p*-OMe)C_6H_4I	high	44
2		(*p*-NO_2)C_6H_4I	small	12
3		PhBr	high	16
4		PhCl	trace	0
5	**1a** to PhI ratio	1:1	high	43
6		1:2	high	31
7	$Pd(OAc)_2$ loading	5 mol %	trace	<1
8		10 mol %	trace	1
9		50 mol %	average	20
10	azolium salt	**1b**	average	56
11		**1c**	average	34

[a]ESI-MS, $I = I_{[NHC\text{-}Ph]+}/I_{[NHC\text{-}Me]+}$, where $0.1 < I < 0.3$, small; $0.3 < I < 0.5$, average; and $I > 1$, high. [b]After 24 h of heating.

mentioned. The use of aryl halides with electron-donating substituents favors the target product formation (Table 1, entry 1), whereas the use of aryl halides with electron-withdrawing substituents is disadvantageous for the process (Table 1, entry 2). The observed yields correlate with Hammett parameters. The use of aryl bromides results in reduced yields of **2a** (Table 1, entry 3), whereas nonactivated aryl chlorides are totally nonreactive in the R−NHC exchange (Table 1, entry 4). The proportion of starting reagents has no significant influence on the reaction (Table 1, entries 5 and 6). Reduced loads of palladium result in substantial decrease in the yields of the final product (Table 1, entries 7−9). The scope of reversible R−NHC coupling also includes imidazolium salts with bulky substituents on nitrogen, e.g., 1,3-dimesityl-1*H*-imidazol-3-ium iodide (**1b**) and 1,3-bis(2,6-diisopropylphenyl)-1*H*-imidazol-3-ium iodide (**1c**) (Table 1, entries 10 and 11).

Possible Mechanism of R,R′−NHC Exchange. For a better insight into the mechanism, a potential energy surface was calculated for the studied system. The mechanism of the process, resulting in the exchange of organic substituents on the carbene carbon, was analyzed at PBE1PBE/6-311G(d) &def2TZVP D3BJ level. As long as palladium acetate is invariably reduced under the action of DMF, Pd(0) species **4** were chosen as a starting point (Figure 6). Complex **4** coordinates the initial azolium salt **1a** and forms a prereaction complex **5**. This stage is exothermic ($\Delta E_{4\to5}$ = −15.4 kcal/mol) even though the iodide ion remains in the outer sphere of the complex and is not coordinated directly to the palladium atom (Figure 6). The next stage, oxidative addition of the azolium salt via transition state **6-TS**, is exothermic ($\Delta E_{5\to7}$ = −24.6 kcal/mol) and has a low activation energy ($\Delta E^{\ddagger}_{5\to6\text{-}TS}$ = 16.0 kcal/mol). In product **7**, coordination sphere of palladium atom contains the methyl group, the NHC-ligand and two DMF molecules, whereas the iodide-ion is located in the outer sphere and coordinated by a single H-bond to a formamide hydrogen of DMF. Subsequent rearrangement of complex **7**, associated with the elimination of one DMF molecule and the transfer of iodide-ion to coordination sphere of palladium, is accompanied by a small increase in energy $\Delta E_{7\to8}$ = 4.4 kcal/mol. The next step, oxidative addition of aryl halide (PhI) via transition state **9-TS**, yields octahedral Pd(IV) complex **10**. Activation energy for this step, $\Delta E^{\ddagger}_{8\to9\text{-}TS}$= 16.5 kcal/mol, is similar to activation energy for the first oxidative addition of azolium salt. In screening for the most stable isomer of complex **10**, the isomer with phenyl group and NHC-ligand in *trans* was found to be relatively unstable; it undergoes rearrangement into a significantly more stable complex **10b** with phenyl group and NHC-ligand in the *cis*-position (Figures 6, S35). Subsequent transformation may involve either of two channels. The first of them is reductive elimination of MeI molecule via transition state **11-TS** with activation energy $\Delta E^{\ddagger}_{10b\to11\text{-}TS}$ = 18.6 kcal/mol. Transition state **11-TS** promotes the transfer of methyl group from palladium onto iodine, whereas DMF molecule essentially loses its bonding with the metal atom. Complex **12**, the formation of which is exothermic ($\Delta E_{10b\to12}$ = −12.4 kcal/mol), has square planar geometry with MeI molecule coordinated to the metal.

The alternative reaction channel, Ph−NHC coupling, involves transition state **13-TS** with activation energy $\Delta E^{\ddagger}_{10b\to13\text{-}TS}$ = 25.7 kcal/mol leading to product **14** where the Ph−NHC fragment is detached from the metal atom. Formation of complex **14** is strongly exothermic ($\Delta E_{10b\to14}$ = −31.3 kcal/mol). Whereas subsequent elimination of the MeI molecule is kinetically unfavorable ($\Delta E^{\ddagger}_{14\to15\text{-}TS}$ = 39.3 kcal/mol). Despite the fact that in products **12** and **14** the palladium atom is in a similar square planar environment of ligands (organic substituent, two iodine atoms and a neutral ligand molecule: NHC in **12** or DMF in **14**) the energy of complex **14** is by 18.9 kcal/mol lower than the energy of complex **12**. Thus, assuming the formation of Pd(IV) complex as a key intermediate, it can be suggested that both processes, MeI elimination and Ph−NHC coupling, are in principle accessible. Formation of MeI is possible at lower temperatures but involves formation of less favorable intermediate, whereas the direct Ph−NHC coupling requires higher temperatures, but results in the most stable reaction product in the studied system (**14**).

DOI: 10.1021/acs.inorgchem.9b01630
Inorg. Chem. XXXX, XXX, XXX−XXX

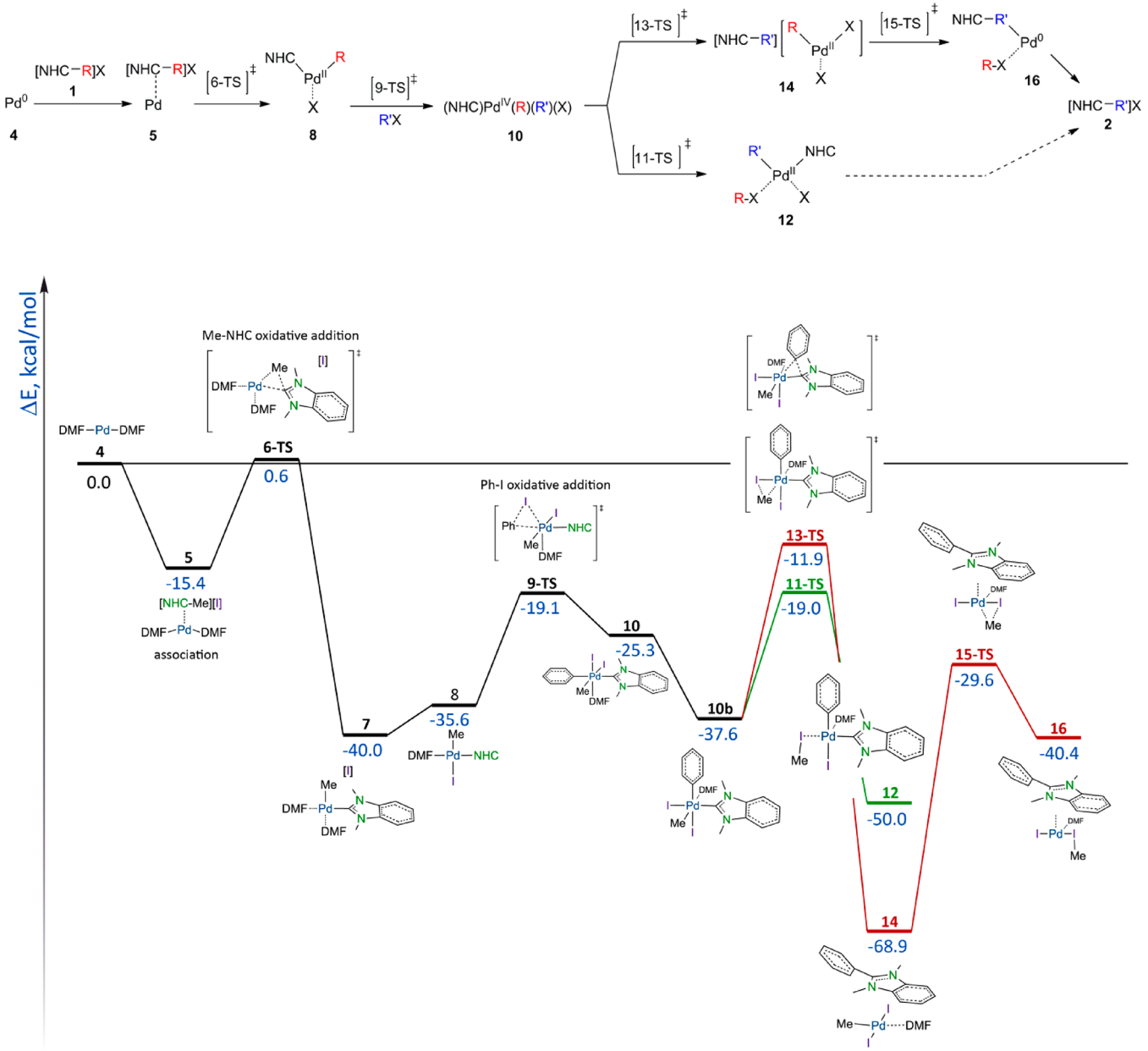

Figure 6. Calculated potential energy profile of the Me-NHC/Ph−NHC exchange reaction at PBE1PBE/6-311G(d)&def2TZVP D3BJ level (see Supporting Information for a description of the model system).

It should be noted that a number of different pathways were analyzed in the present study by theoretical calculations (Supporting Information, section 5). The route of oxidative addition via dipalladium complex was found less probable (Supporting Information, Scheme S1 and discussion therein). The transfer of methyl group between palladium atoms in binuclear complex is characterized by a high activation energy of 41.7 kcal/mol (Figures S28−S30). Formation of Pd(IV) complex through addition of Me-NHC^{+}I^{-} salt to Pd(II) complex is also kinetically unlikely. The Me-NHC oxidative addition step with Pd(IV) complex formation has rather high activation energy of 63.3 kcal/mol (Figures S31−S33). In addition, the R,R′−NHC coupling mechanism involving MeI elimination was considered; however, it is also characterized by a high potential barrier of 46.2 kcal/mol (Figures S36−S38). Thus, the most probable mechanism for R,R′-exchange combines oxidative addition of Me-NHC^{+}I^{-} to Pd(0) complex with subsequent oxidative addition of PhI leading to formation of Pd(IV) complex (Figure 6).

Of course, the theoretical study represents only a model of the metal center and involves certain simplifications. The real experimental system is much more complex (i.e., in the structure of metal center, colloidal organization, etc.). Nevertheless, in spite of model character, the calculations performed are in good agreement with the experimental findings. Computational modeling provides rational pathway for the R,R′−NHC exchange process. It is important to emphasize that the computed energy surface is consistent with the formation of MeI observed experimentally.

R,R′−NHC Coupling and Leaching Involving Pd NPs. Pd NPs were first isolated in neat form (Figure S25, Supporting Information) and then used in the reaction. Under the same experimental conditions (Scheme 3), R,R′−NHC coupling was carried out using presynthesized palladium

DOI: 10.1021/acs.inorgchem.9b01630
Inorg. Chem. XXXX, XXX, XXX−XXX

nanoparticles and **1a**. After 24 h the product **2a** was detected in the reaction mixture by ESI-MS (m/z 223) and ^{1}H NMR (signal at δ 3.89 ppm). The reaction was also performed with azolium salts **1b** and **1c**, where the formation of corresponding products **2b** and **2c** was detected by ESI-MS. Although the activity of isolated nanoparticles may be lower compared to the nanoparticles formed *in situ* (partial deactivation and agglomeration may occur during isolation), the obtained results clearly indicated the possibility of the studied reaction involving Pd NPs.

Detailed ESI-MS study of the reaction mixture revealed Pd-containing complex in solution upon the reaction of Pd NPs with **1a**. Plausible structure includes two NHC moieties and one Pd atom. The number of Pd atoms can be clearly established according to simulation of the isotopic distribution (Figure 7) and the presence of NHC moieties was confirmed

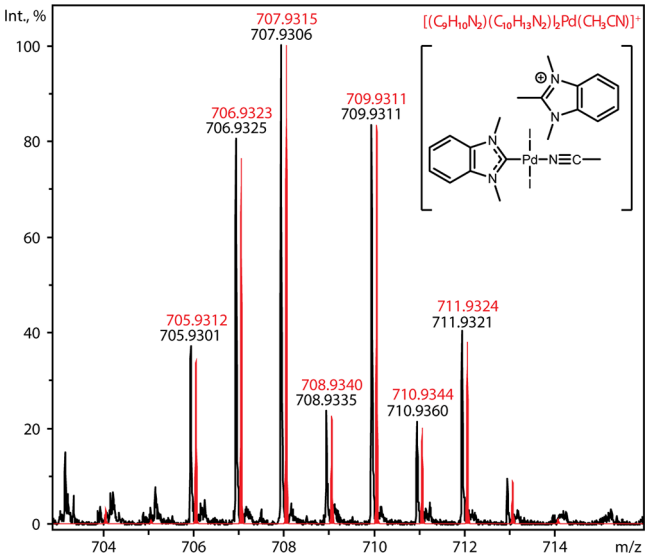

Figure 7. ESI-(+)MS spectrum of the detected Pd-containing ion, formed as a result of interaction of salt **1a** with Pd NPs after 10 min (3 μmol **1a**, Pd NPs prepared from 3 μmol of Pd(OAc)$_2$, DMF, 140 °C). Experimental spectrum is shown in black, and the theoretical simulation is shown in red.[12]

by MS^2 experiment (Figure S23, Supporting Information). A possible structure of the ion was proposed according to quantum chemical modeling (Figure S39). Appearance of Pd-NHC framework in the mononuclear metal complex provides the evidence of C−C bond breakage in **1a** salt under the influence of Pd NPs. These findings further support the hypothesis shown in Scheme 1B.

To the best of our knowledge, this is the first example of metal leaching from Pd NPs initiated by NHC ligand core. Transfer of metal atoms from Pd nanoparticles to solution and formation of Pd/NHC complex can be proposed on the bases of the experiment.

CONCLUSIONS

The present study reports experimental evidence of Pd insertion into C−C bond in a chemical system with R−NHC$^+$ molecular framework. The results indicate plausibility of breaking of the C−C bond in R−NHC$^+$X$^-$ azolium salt under studied conditions, which is a key requirement for reversibility of the R−NHC coupling process. A model reaction of 2-substituted azolium salts with aryl halides of various nature in the presence of palladium leads to substituent exchange on the carbene carbon atom. The reaction is tolerant to modified substrates and conditions.

Computational study indicates that the trapping process preferentially proceeds via Pd(IV) complex formed stepwise by double oxidative addition of the starting azolium salt and aryl halide. The organic substituent exchange is possible when the groups were present simultaneously in coordination sphere of the metal. Thus, Pd(IV) complex encompassing both methyl and phenyl substituents is an important intermediate of the process. Decomposition of the Pd(IV) complex may proceed in two ways; both are accompanied by elimination of a MeI molecule detected experimentally. Decomposition of the Pd(IV) complex may begin with the Ph−NHC coupling followed by MeI elimination. However, this channel leads to a very stable intermediate which makes the subsequent elimination of organic halide kinetically unfavorable. The alternative decomposition channel of the Pd(IV) complex with MeI elimination followed by Ph−NHC coupling is more likely as it is not accompanied by formation of a kinetically blocked intermediate. In both cases, regardless of the reaction channel, the overall pathway is shifted toward Ph−NHC coupling product which has lower energy as compared to the Pd(II) alkyl complex.

Using presynthesized Pd NPs reversibility of R,R′−NHC coupling was experimentally demonstrated. Leaching of NHC-containing Pd complex from the surface of Pd nanoparticle was observed upon reaction with azlolium salts, which provides an evidence for the nano-to-molecular transformation in the studied system.

NHCs are well-known ligands for transition metal catalysis. Metal systems with NHC ligands can switch their state from molecular (represented by metal complexes) to nanoscale (represented by metal clusters and nanoparticles). Such transitions have been commonly associated with decomposition of M/NHC catalysts via R−NHC coupling. However, the possibility of reverse transition (by C−C bond activation in R−NHC$^+$X$^-$ azolium salts) has not been studied for the M/NHC systems. This article provides the first demonstration of possibility of such reverse transition which may well provide a key to construction of dynamic cocktail-type Pd/NHC systems.

Indeed, understanding mechanistic pathways associated with R−NHC coupling is required for rational catalyst design, as discussed above (see Introduction). Typically, it is assumed that C−C bond oxidative addition to metal centers is an endothermic process accompanied by overcoming of high activation barriers. Here, we demonstrate that oxidative addition of C−C bond in the R−NHC$^+$X$^-$ species has surprisingly small activation barriers and the process is noticeably exothermic (**I** → **II-TS** → **III** and **VI** → **V-TS** → **IV**, Scheme 2). This unique feature provides the necessary basement for the studied transformation of Pd-active species. Moreover, the findings go far beyond the studied system and open possibilities for catalytic C−C bond activations (usually rather difficult to achieve) in the revealed molecular framework.

EXPERIMENTAL SECTION

General Considerations. ^{1}H and ^{13}C{^{1}H} NMR spectra were recorded on a Bruker Fourier 300HD instrument at 300 MHz for ^{1}H and at 75 MHz for 13C{^{1}H}. ^{1}H and ^{13}C{^{1}H} chemical shifts are

DOI: 10.1021/acs.inorgchem.9b01630
Inorg. Chem. XXXX, XXX, XXX−XXX

given in ppm relative to the residual peak of the solvent for the proton spectra (δ 2.75 ppm, δ 2.92 ppm, δ 8.03 ppm for DMF-d_7 and δ 2.50 ppm for DMSO-d_6) and for the carbon spectra (δ 163.2 ppm, δ 34.9 ppm, δ 29.8 ppm for DMF-d_7 and δ 39.52 ppm for DMSO-d_6). GC-MS measurements were carried out on Agilent 7890 gas chromatograph with Agilent 5970 mass-selective detector. Measurements were performed in scan range from m/z 80 to m/z 300 mode with ionization energy set at 70 eV, source temperature set at 230 °C and transfer capillary temperature set at 300 °C. Separation was carried out on Agilent HP-5MS fused silica capillary column (30 m length; 250 μm I.D.; 0.25 μm film thickness, (5% phenyl)-methylpolysiloxane) using He (5.0 grade, NII KM) as carrier gas at flow of 0.5 mL/min. The temperature program was started at 40 °C and held for 3 min, then increased at a rate of 5 °C/min to 60 °C, and then increased at a rate of 25 °C/min to 160 °C and held for 1 min. Injection port temperature was set at 300 °C and was operated in split mode at 15:1 ratio with sample injection volume of 10 μL. The spectra were processed using the Bruker Data Analysis 4.0 software package with NIST 14 spectra database.

High-resolution mass spectra were registered on Bruker maXis Q-TOF instrument equipped with electrospray ionization (ESI) ion source. The measurements were performed in positive mode with HV capillary at 4.5 kV, spray shield offset at −0.5 kV, and scan range of m/z 50−1200. External calibration was performed using low-concentration tuning mix solution (Agilent Technologies). Direct syringe injection was used for all analyzed solutions in MeCN at flow rate of 5 μL/min. Nitrogen was used as both nebulizer gas at 1 bar and dry gas at 4.0 L/min, 200 °C. Nitrogen (6.0 grade, NII KM) was used as collision gas for MS^2 experiments. MS^2 spectrum was acquired at 0.08 Hz and precursor was isolated with a width of 7 Da. Collision energies were set to 20 eV, data was acquired for 1 min in the range 100−1500 m/z. All recorded spectra were processed using Bruker Data Analysis 4.0 software package.

All synthetic manipulations were conducted under argon atmosphere using standard Schlenk techniques. Dry solvents were used for all operations. Column chromatography was conducted on Al_2O_3 (Brockmann II, neutr.). Glassware was dried at 120 °C in an oven for at least 3 h.

1,2,3-Trimethyl-1*H*-benzimidazol-3-ium iodide,[13] 1,3-dimethyl-2-phenyl-1*H*-benzimidazol-3-ium iodide,[14] 1,3-dimesityl-2-methyl-1*H*-imidazol-3-ium iodide,[15] 1,3-bis(2,6-diisopropylphenyl)-2-methyl-1*H*-imidazol-3-ium,[15] and 1,3-dimethyl-1*H*-benzimidazol-3-ium iodide[16] were synthesized as described in the literature. All other chemicals were purchased from commercial sources.

1,2,3-Trimethyl-1*H*-benzimidazol-3-ium iodide (1a). Phenylenediamine (0.019 mol, 2.0 g) and acetic acid (0.062 mol, 3.53 mL) were placed in a 25 mL round-bottom flask with magnetic stir bar. Reaction mixture was refluxed for 2 h. Then, ice and KOH were added up to pH 10, and a light-purple solid was filtered out and was purified by recrystallization from water. Isolated as a light-yellow needle-shaped crystals, 2-methylbenzimidazole (1.72 g, yield 70%) was used in the next step. 2-Methylbenzimidazole (0.005 mol, 0.66 g), 12 mL of benzene, and MeI (0.015 mol, 0.93 mL) were added to solution of Na (0.005 mol, 0.12 g) in 2 mL of ethanol under constant stirring and refluxed for 18 h. The reaction mixture was then cooled to the room temperature, and the solvent was removed. The crude product was purified by recrystallization from 95% ethanol. The desired product (**1a**) was isolated as colorless needle-shaped crystals (1.15 g, 80% yield). ^{1}H NMR (300 MHz, DMSO-d_6), δ, ppm: 7.97−8.00 (m, 2H), 7.62−7.65 (m, 2H), 4.00 (s, 6H), 2.88 (s, 3H). $^{13}C\{^1H\}$ NMR (75 MHz, DMSO-d_6) δ ppm: 152.2, 131.3, 125.8, 112.7, 31.7, 10.6. ESI-MS: $[M - I]^+$ calcd for $[C_{10}H_{13}N_2]^+$, m/z 161.1073; found, m/z 161.1076 (Δ = 1.9 ppm). Anal. Calcd for $C_{10}H_{13}IN_2$: C, 41.69; H, 4.55; N, 9.72. Found: C, 41.66; H, 4.56; N, 9.65.

1,3-Dimethyl-2-phenyl-1*H*-benzimidazol-3-ium iodide (2a). 1,3-Dimethyl-1*H*-benzimidazolium iodide[16] (0.001 mol, 274.0 mg), phenyl iodide (0.002 mol, 408.0 mg), Cu_2O (29.0 mg, 20 mol %), and NaOAc (0.001 mol, 82.0 mg) in DMF solution (5 mL) were placed in a Schlenk tube and kept at 120 °C for 24 h under constant stirring in argon atmosphere. The reaction mixture was then cooled down to room temperature, solvent was removed, and the desired product (**2a**) was isolated by column chromatography, using dichloromethane/methanol (v/v, 100/1−20/1) as eluent. Yield: 0.263 g (75%). ^{1}H NMR (300 MHz, DMSO-d_6), δ, ppm: 8.13−8.16 (m, 2H), 7.91−7.93 (m, 2H), 7.75−7.85 (m, 5H), 3.90 (s, 6H). $^{13}C\{^1H\}$ NMR (75 MHz, DMSO-d_6), δ, ppm: 150.3, 132.9, 131.7, 130.8, 129.4, 126.6, 121.0, 113.4, 32.8. ESI-MS: $[M - I]^+$ calcd for $[C_{15}H_{15}N_2]^+$, m/z 223.1230; found, m/z 223.1227 (Δ = 1.3 ppm). Anal. Calcd for $C_{15}H_{15}IN_2$: C, 51.45; H, 4.32; N, 8.00. Found: C, 51.38; H, 4.27; N, 7.94.

General Procedure for Analytical Assessment of the Oxidative Addition of R−NHC to Metal by Mass Spectrometry and NMR and Quantitative Isolation of the R−NHC Coupling Product. A screw-top tube equipped with magnetic stir bar was charged with 2-methylation azolium salt (0.1 mmol) in 500 μL of DMF; the inside of the tube was thoroughly flushed with argon, then ArX (0.2 mmol) and metal source (0.1 mmol) were added. The reaction mixture was thoroughly flushed with argon, sealed, and heated at 140 °C under continuous magnetic stirring. After 24 h, the reaction was stopped and the mixture was analyzed by mass-spectrometry and ^{1}H NMR. Product **2a** was quantitatively isolated from the reaction mixture by flash chromatography after evaporation of the solvent. The mixture was passed through a column (h = 3 cm, d = 2.5 cm) packed with alumina (Brockmann II, neutr.), with gradient elution using DCM−MeOH (100/1 to 20/1, v/v). The pure product was obtained as colorless crystals (yield 20%). The structure was confirmed by ^{1}H NMR (300 MHz, DMSO-d_6), δ, ppm: 8.12−8.15 (m, 2H), 7.91−7.93 (m, 2H), 7.75−7.85 (m, 5H), 3.89 (s, 6H). $^{13}C\{^1H\}$ NMR (75 MHz, DMSO-d_6), δ, ppm: 150.3, 132.9, 131.7, 130.8, 129.4, 126.6, 121.0, 113.4, 32.8. ESI-MS: $[M - I]^+$ calcd for $[C_{15}H_{15}N_2]^+$, m/z 223.1230; found, m/z 223.1230 (Δ = 0.2 ppm). Anal. Calcd for $C_{15}H_{15}IN_2$: C, 51.45; H, 4.32; N, 8.00. Found: C, 51.38; H, 4.27; N, 7.94.

Synthesis of Compounds 1b and 1c. In a 25 mL round-bottom flask with magnetic stir bar, 1,3-bis(2,6-diisopropylphenyl)-imidazolium chloride[17] (0.001 mol, 0.42 g) or 1,3-dimesityl-1*H*-imidazol-3-ium chloride[17] (0.001 mol, 0.34 g) in THF solution (5 mL) was cooled to −78 °C. *n*-BuLi (0.483 mL, 1.14 mmol, 1.6 M solution in hexanes) was added dropwise to get a white suspension. The reaction mixture was stirred for 10 min. The resulting clear solution was warmed to room temperature and stirred for another 5 min, and then MeI (0.0011 mmol, 0.09 mL) was added at −78 °C. A white precipitate was isolated by filtration and then washed with water and hexane and dried. The desired products (**1b** and **1c**) were isolated as colorless solids.

*1,3-Dimesityl-2-methyl-1H-imidazol-3-ium iodide (**1b**).* Yield: 0.280 g (63%). ^{1}H NMR (300 MHz, DMF-d_7), δ, ppm: 8.31 (s, 2H), 7.29 (s, 4H), 2.42 (s, 6H), 2.39 (s, 3H), 2.17 (s, 12H). $^{13}C\{^1H\}$ NMR (75 MHz, DMF-d_7), δ, ppm: 149.0, 146.3, 141.6, 135.1, 130.1, 124.4, 20.7, 16.9, 9.5. ESI-MS: $[M - I]^+$ calcd for $[C_{22}H_{27}N_2]^+$, m/z 319.2169; found, m/z 319.2166 (Δ = 0.9 ppm).

*1,3-Bis(2,6-diisopropylphenyl)-2-methyl-1H-imidazol-3-ium (**1c**).* Yield: 0.269 g (51%). ^{1}H NMR (300 MHz, DMF-d_7), δ, ppm: 8.62 (d, J = 3.7 Hz, 2H), 7.83−7.76 (m, 2H), 7.65 (dd, J = 7.8, 3.7 Hz, 4H), 2.46−2.36 (m, 4H), 2.34 (s, 3H), 1.37−1.25 (m, 24H). $^{13}C\{^1H\}$ NMR (75 MHz, DMSO-d_6), δ, ppm: 150.1, 147.0, 145.5, 132.6, 129.9, 125.6, 24.9, 24.1, 22.8, 22.3, 10.6. ESI-MS: $[M - I]^+$ calcd for $[C_{28}H_{39}N_2]^+$, m/z 403.3108; found, m/z 403.3111 (Δ = 0.7 ppm). Anal. Calcd for $C_{28}H_{39}IN_2$: C, 63.39; H, 7.41; N, 5.28. Found: C, 63.37; H, 7.49; N, 5.36.

Computational Details. Reagents, products, intermediates, and transition states **4**−**16** were fully optimized by PBE1PBE[18] with basis sets 6-311G(d)[19] for H, C, N, and O and def2TZVP[20] for Pd and I. The dispersion was accounted for by using Grimme D3BJ empirical corrections.[21]

Several benchmark studies have shown that the PBE1PBE (aka PBE0) method is reliable and accurate for modeling reactions involving late transition metals, including palladium. In particular, it was shown that for model reactions of C−C, C−Hal, and C−H

DOI: 10.1021/acs.inorgchem.9b01630
Inorg. Chem. XXXX, XXX, XXX−XXX

oxidative addition to the Pd center, the root-mean-square (RMSD) deviation for this method is only 0.8 kcal/mol when compared with the CCSD(T) method.[22] For a larger range of oxidative addition reactions (C−H, C−C, O−H, B−H, N−H, C−Cl) to the Pd center, it was shown that the most accurate method is the PBE1PBE D3, for which the mean absolute deviation (MAD) is 1.1 kcal/mol.[23]

Vibrational spectra were calculated for all optimized molecules to determine the types of stationary points on the potential energy surface. All computations were performed in the Gaussian 16 software package.[24]

■ ASSOCIATED CONTENT

Supporting Information

The Supporting Information is available free of charge on the ACS Publications website at DOI: 10.1021/acs.inorgchem.9b01630.

Additional experimental data, NMR spectra, ESI-MS data, TEM images, and a detailed description of theoretical calculations (PDF)

■ AUTHOR INFORMATION

Corresponding Author

*E-mail (V.P.A.): val@ioc.ac.ru.

ORCID

Ekaterina A. Denisova: 0000-0003-4818-2942
Dmitry B. Eremin: 0000-0003-2946-5293
Evgeniy G. Gordeev: 0000-0002-0545-5720
Andrey M. Tsedilin: 0000-0001-6483-0327
Valentine P. Ananikov: 0000-0002-6447-557X

Notes

The authors declare no competing financial interest.

■ ACKNOWLEDGMENTS

This research was supported by the Russian Science Foundation (RSF) Grant 17-13-01526. The authors also thank Alexey S. Galushko for microscopy services.

■ REFERENCES

(1) (a) Hopkinson, M. N.; Richter, C.; Schedler, M.; Glorius, F. An Overview of N-Heterocyclic Carbenes. *Nature* **2014**, *510*, 485−496. (b) Díez-González, S.; Marion, N.; Nolan, S. P. N-Heterocyclic Carbenes in Late Transition Metal Catalysis. *Chem. Rev.* **2009**, *109*, 3612−3676. (c) Fortman, G. C.; Nolan, S. P. N-Heterocyclic Carbene (NHC) Ligands and Palladium in Homogeneous Cross-Coupling Catalysis: a Perfect Union. *Chem. Soc. Rev.* **2011**, *40*, 5151−5169. (d) Valente, C.; Çalimsiz, S.; Hoi, K. H.; Mallik, D.; Sayah, M.; Organ, M. G. The Development of Bulky Palladium NHC Complexes for the Most-Challenging Cross-Coupling Reactions. *Angew. Chem., Int. Ed.* **2012**, *51*, 3314−3332. (e) Herrmann, W. A. N-Heterocyclic Carbenes: A New Concept in Organometallic Catalysis. *Angew. Chem., Int. Ed.* **2002**, *41*, 1290−1309. (f) Nasr, A.; Winkler, A.; Tamm, M. Anionic N-Heterocyclic Carbenes: Synthesis, Coordination Chemistry and Applications in Homogeneous Catalysis. *Coord. Chem. Rev.* **2016**, *316*, 68−124. (g) Peris, E. Smart N-Heterocyclic Carbene Ligands in Catalysis. *Chem. Rev.* **2018**, *118*, 9988−10031. (h) Hazari, N.; Melvin, P. R.; Beromi, M. M. Well-Defined Nickel and Palladium Precatalysts for Cross-Coupling. *Nat. Rev. Chem.* **2017**, *1*, No. 0025. (i) Hameury, S.; de Frémont, P.; Braunstein, P. Metal Complexes with Oxygen-Functionalized NHC Ligands: Synthesis and Applications. *Chem. Soc. Rev.* **2017**, *46*, 632−733.

(2) (a) Díez-González, S.; Nolan, S. P. Stereoelectronic Parameters Associated with N-Heterocyclic Carbene (NHC) ligands: A Quest for Understanding. *Coord. Chem. Rev.* **2007**, *251*, 874−883. (b) Nelson, D. J.; Nolan, S. P. Quantifying and Understanding the Electronic Properties of N-Heterocyclic Carbenes. *Chem. Soc. Rev.* **2013**, *42*, 6723−6753.

(3) (a) Beletskaya, I. P.; Cheprakov, A. V. The Heck Reaction as a Sharpening Stone of Palladium Catalysis. *Chem. Rev.* **2000**, *100*, 3009−3066. (b) Fürstner, A. Olefin Metathesis and Beyond. *Angew. Chem., Int. Ed.* **2000**, *39*, 3012−3043. (c) Littke, A. F.; Fu, G. C. Palladium-Catalyzed Coupling Reactions of Aryl Chlorides. *Angew. Chem., Int. Ed.* **2002**, *41*, 4176−4211. (d) Kantchev, E. A. B.; O'Brien, C. J.; Organ, M. G. Palladium Complexes of N-Heterocyclic Carbenes as Catalysts for Cross-Coupling Reactions a Synthetic Chemist's Perspective. *Angew. Chem., Int. Ed.* **2007**, *46*, 2768−2813. (e) Würtz, S.; Glorius, F. Surveying Sterically Demanding N-Heterocyclic Carbene Ligands with Restricted Flexibility for Palladium-Catalyzed Cross-Coupling Reactions. *Acc. Chem. Res.* **2008**, *41*, 1523−1533. (f) Samojłowicz, C.; Bieniek, M.; Grela, K. Ruthenium-Based Olefin Metathesis Catalysts Bearing N-Heterocyclic Carbene Ligands. *Chem. Rev.* **2009**, *109*, 3708−3742. (g) Lin, J. C. Y.; Huang, R. T. W.; Lee, C. S.; Bhattacharyya, A.; Hwang, W. S.; Lin, I. J. B. Coinage Metal−N-Heterocyclic Carbene Complexes. *Chem. Rev.* **2009**, *109*, 3561−3598. (h) Vougioukalakis, G. C.; Grubbs, R. H. Ruthenium-Based Heterocyclic Carbene-Coordinated Olefin Metathesis Catalysts. *Chem. Rev.* **2010**, *110*, 1746−1787. (i) Dröge, T.; Glorius, F. The Measure of All Rings − N-Heterocyclic Carbenes. *Angew. Chem., Int. Ed.* **2010**, *49*, 6940−6952. (j) Johansson Seechurn, C. C. C.; Kitching, M. O.; Colacot, T. J.; Snieckus, V. Palladium-Catalyzed Cross-Coupling: a Historical Contextual Perspective to the 2010 Nobel Prize. *Angew. Chem., Int. Ed.* **2012**, *51*, 5062−5085. (k) Li, H.; Johansson Seechurn, C. C. C.; Colacot, T. J. Development of Preformed Pd Catalysts for Cross-Coupling Reactions, Beyond the 2010 Nobel Prize. *ACS Catal.* **2012**, *2*, 1147−1164. (l) Wang, F.; Liu, L.-J.; Wang, W.; Li, S.; Shi, M. Chiral NHC−Metal-Based Asymmetric Catalysis. *Coord. Chem. Rev.* **2012**, *256*, 804−853. (m) Gildner, P. G.; Colacot, T. J. Reactions of the 21st Century: Two Decades of Innovative Catalyst Design for Palladium-Catalyzed Cross-Couplings. *Organometallics* **2015**, *34*, 5497−5508.

(4) Cavell, K. N-Heterocyclic Carbenes/Imidazolium Salts as Substrates in Catalysis: The catalytic 2-Substitution and Annulation of Heterocyclic Compounds. *Dalton Trans.* **2008**, *0*, 6676−6685.

(5) (a) McGuinness, D. S.; Green, M. J.; Cavell, K. J.; Skelton, B. W.; White, A. H. Synthesis and Reaction Chemistry of Mixed Ligand Methylpalladium−Carbene Complexes. *J. Organomet. Chem.* **1998**, *565*, 165−178. (b) McGuinness, D. S.; Cavell, K. J.; Skelton, B. W.; White, A. H. Zerovalent Palladium and Nickel Complexes of Heterocyclic Carbenes: Oxidative Addition of Organic Halides, Carbon−Carbon Coupling Processes, and the Heck Reaction. *Organometallics* **1999**, *18*, 1596−1605. (c) McGuinness, D. S.; Cavell, K. J. Reaction of CO with a Methylpalladium Heterocyclic Carbene Complex: Product Decomposition Routes Implications for Catalytic Carbonylation Processes. *Organometallics* **2000**, *19*, 4918−4920. (d) McGuinness, D. S.; Cavell, K. J.; Yates, B. F.; Skelton, B. W.; White, A. H. Oxidative Addition of the Imidazolium Cation to Zerovalent Ni, Pd, and Pt: A Combined Density Functional and Experimental Study. *J. Am. Chem. Soc.* **2001**, *123*, 8317−8328. (e) Caddick, S.; Cloke, F. G. N.; Hitchcock, P. B.; Leonard, J.; Lewis, A. K. d. K.; McKerrecher, D.; Titcomb, L. R. The First Example of Simple Oxidative Addition of an Aryl Chloride to a Discrete Palladium N-Heterocyclic Carbene Amination Precatalyst. *Organometallics* **2002**, *21*, 4318−4319. (f) Cavell, K. J.; McGuinness, D. S. Redox Processes Involving Hydrocarbylmetal (N-Heterocyclic Carbene) Complexes and Associated Imidazolium Salts: Ramifications for Catalysis. *Coord. Chem. Rev.* **2004**, *248*, 671−681. (g) Clement, N. D.; Cavell, K. J.; Ooi, L.-l. Zerovalent N-Heterocyclic Carbene Complexes of Palladium and Nickel Dimethyl Fumarate: Synthesis, Structure, and Dynamic Behavior. *Organometallics* **2006**, *25*, 4155−4165. (h) Nielsen, D. J.; Cavell, K. J.; Skelton, B. W.; White, A. H. Methyl-Palladium(II) Complexes of Pyridine-Bridged Bis(Nucleophilic Heterocyclic Carbene) Ligands: Substituent Effects on Structure, Stability, and Catalytic Performance. *Inorg. Chim. Acta* **2006**, *359*, 1855−1869. (i) Graham, D. C.; Cavell, K. J.; Yates, B. F.

DOI: 10.1021/acs.inorgchem.9b01630
Inorg. Chem. XXXX, XXX, XXX−XXX

Oxidative Addition of 2-Substituted Azolium Salts to Group-10 Metal Zero Complexes − A DFT Study. *Dalton Trans.* **2007**, *0*, 4650−4658. (j) Magill, A. M.; Yates, B. F.; Cavell, K. J.; Skelton, B. W.; White, A. H. Synthesis of N-Heterocyclic Carbene Palladium (II) Bis-Phosphine Complexes and Their Decomposition in the Presence of Aryl Halides. *Dalton Trans.* **2007**, *0*, 3398−3406. (k) Normand, A. T.; Nechaev, M. S.; Cavell, K. J. Mechanisms in the Reaction of Palladium(II)−π-Allyl Complexes with Aryl Halides: Evidence for NHC Exchange Between Two Palladium Complexes. *Chem. - Eur. J.* **2009**, *15*, 7063−7073. (l) Couzijn, E. P. A.; Zocher, E.; Bach, A.; Chen, P. Gas-Phase Energetics of Reductive Elimination from a Palladium(II) N-Heterocyclic Carbene Complex. *Chem. - Eur. J.* **2010**, *16*, 5408−5415.

(6) (a) Astakhov, A. V.; Khazipov, O. V.; Chernenko, A. Y.; Pasyukov, D. V.; Kashin, A. S.; Gordeev, E. G.; Khrustalev, V. N.; Chernyshev, V. M.; Ananikov, V. P. A New Mode of Operation of Pd-NHC Systems Studied in a Catalytic Mizoroki−Heck Reaction. *Organometallics* **2017**, *36*, 1981−1992. (b) Gordeev, E. G.; Ananikov, V. P. Switching the Nature of Catalytic Centers in Pd/NHC Systems by Solvent Effect Driven Non-Classical R−NHC Coupling. *J. Comput. Chem.* **2019**, *40*, 191−199. (c) Chernyshev, V. M.; Khazipov, O. V.; Shevchenko, M. A.; Chernenko, A. Y.; Astakhov, A. V.; Eremin, D. B.; Pasyukov, D. V.; Kashin, A. S.; Ananikov, V. P. Revealing the unusual role of bases in activation/deactivation of catalytic systems: O−NHC coupling in M/NHC catalysis. *Chem. Sci.* **2018**, *9*, 5564−5577.

(7) Gordeev, E. G.; Eremin, D. B.; Chernyshev, V. M.; Ananikov, V. P. Influence of R−NHC Coupling on the Outcome of R−X Oxidative Addition to Pd/NHC Complexes (R = Me, Ph, Vinyl, Ethynyl). *Organometallics* **2018**, *37*, 787−796.

(8) Eremin, D. B.; Ananikov, V. P. Understanding Active Species in Catalytic Transformations: from Molecular Catalysis to Nanoparticles, Leaching, "Cocktails" of Catalysts and Dynamic Systems. *Coord. Chem. Rev.* **2017**, *346*, 2−19.

(9) (a) Tran, B. L.; Fulton, J. L.; Linehan, J. C.; Lercher, J. A.; Bullock, R. M. Rh(CAAC)-Catalyzed Arene Hydrogenation: Evidence for Nanocatalysis and Sterically Controlled Site-Selective Hydrogenation. *ACS Catal.* **2018**, *8*, 8441−8449. (b) Tran, B. L.; Fulton, J. L.; Linehan, J. C.; Balasubramanian, M.; Lercher, J. A.; Bullock, R. M. Operando XAFS Studies on Rh(CAAC)-Catalyzed Arene Hydrogenation. *ACS Catal.* **2019**, *9*, 4106−4114.

(10) (a) Polynski, M. V.; Ananikov, V. P. Modeling Key Pathways Proposed for the Formation and Evolution of "Cocktail"-Type Systems in Pd-Catalyzed Reactions Involving ArX Reagents. *ACS Catal.* **2019**, *9*, 3991−4005. (b) Kashin, A. S.; Degtyareva, E. S.; Eremin, D. B.; Ananikov, V. P. Exploring the performance of nanostructured reagents with organic-group-defined morphology in cross-coupling reaction. *Nat. Commun.* **2018**, *9*, 2936. (c) Egorova, K. S.; Ananikov, V. P. Toxicity of Metal Compounds: Knowledge and Myths. *Organometallics* **2017**, *36*, 4071−4090.

(11) (a) Meier, M. A. R.; Filali, M.; Gohy, J.-F.; Schubert, U. S. Star-Shaped Block Copolymer Stabilized Palladium Nanoparticles for Efficient Catalytic Heck Cross-Coupling Reactions. *J. Mater. Chem.* **2006**, *16*, 3001−3006. (b) Hashimoto, T.; Tanaka, H.; Koizumi, S.; Naka, K.; Chujo, Y. A Combined Small-Angle Scattering Study of a Chemical Reaction at Specific Sites and Reactioninduced Self-Assembly as a Problem in Open Non-equilibrium Phenomena. *J. Appl. Crystallogr.* **2007**, *40*, s73−s77. (c) Pastoriza-Santos, I.; Liz-Marzán, L. M. N,N-Dimethylformamide as a Reaction Medium for Metal Nanoparticle Synthesis. *Adv. Funct. Mater.* **2009**, *19*, 679−688.

(12) It should be pointed out that the molecular formula detected in the ESI-MS experiment showed the presence of one Pd atom and two NHC residues. The molecular structure given is a possible suggestion only for this formula. A low signal-to-noise ratio was observed, which allows only plausible identification of the complex. Nevertheless, the isotopic pattern was reproduced with a good match, and reliable accuracy was observed (Δ = 1.3 ppm).

(13) Xia, G.; Wu, Z.; Yuan, Y.; Wang, H. The Regioselectivity and Synthetic Mechanism of 1,2-Benzimidazole Squaraines: Combined Experimental and Theoretical Studies. *RSC Adv.* **2013**, *3*, 18055−18061.

(14) Li, S.; Tang, J.; Zhao, Y.; Jiang, R.; Wang, T.; Gao, G.; You, J. Cu-Catalyzed Controllable C−H Mono-/Di-/Triarylations of Imidazolium Salts for Ionic Functional Materials. *Chem. Commun.* **2017**, *53*, 3489−3492.

(15) Ibrahim Al-Rafia, S. M.; Malcolm, A. C.; Liew, S. K.; Ferguson, M. J.; McDonald, R.; Rivard, E. Intercepting Low Oxidation State Main Group Hydrides with a Nucleophilic N-Heterocyclic Olefin. *Chem. Commun.* **2011**, *47*, 6987−6989.

(16) Rubbiani, R.; Kitanovic, I.; Alborzinia, H.; Can, S.; Kitanovic, A.; Onambele, L. A.; Stefanopoulou, M.; Geldmacher, Y.; Sheldrick, W. S.; Wolber, G.; Prokop, A.; Wölfl, S.; Ott, I. Benzimidazol-2-ylidene Gold(I) Complexes are Thioredoxin Reductase Inhibitors with Multiple Antitumor Properties. *J. Med. Chem.* **2010**, *53*, 8608−8618.

(17) Hintermann, L. Expedient Syntheses of the N-Heterocyclic Carbine Precursor Imidazolium Salts IPr·HCl, IMes·HCl and IXy·HCl. *Beilstein J. Org. Chem.* **2007**, *3*, No. 22.

(18) (a) Perdew, J. P.; Burke, K.; Ernzerhof, M. Generalized Gradient Approximation Made Simple. *Phys. Rev. Lett.* **1996**, *77*, 3865−3868. (b) Adamo, C.; Barone, V. Toward Reliable Density Functional Methods without Adjustable Parameters: The PBE0 model. *J. Chem. Phys.* **1999**, *110*, 6158−6170.

(19) (a) Krishnan, R.; Binkley, J. S.; Seeger, R.; Pople, J. A. Self-consistent Molecular Orbital Methods. XX. A Basis Set for Correlated Wave Functions. *J. Chem. Phys.* **1980**, *72*, 650−654. (b) McLean, A. D.; Chandler, G. S. Contracted Gaussian Basis Sets for Molecular Calculations. I. Second Row Atoms, Z = 11−18. *J. Chem. Phys.* **1980**, *72*, 5639−5648.

(20) Weigend, F.; Ahlrichs, R. Balanced Basis Sets of Split Valence, Triple Zeta Valence and Quadruple Zeta Valence Quality for H to Rn: Design and Assessment of Accuracy. *Phys. Chem. Chem. Phys.* **2005**, *7*, 3297−3305.

(21) (a) Grimme, S.; Antony, J.; Ehrlich, S.; Krieg, H. A Consistent and Accurate ab Initio Parametrization of Density Functional Dispersion Correction (DFT-D) for the 94 Elements H-Pu. *J. Chem. Phys.* **2010**, *132*, 154104. (b) Grimme, S.; Ehrlich, S.; Goerigk, L. Effect of the damping function in dispersion corrected density functional theory. *J. Comput. Chem.* **2011**, *32*, 1456−1465.

(22) Quintal, M. M.; Karton, A.; Iron, M. A.; Boese, A. D.; Martin, J. M. L. Benchmark Study of DFT Functionals for Late-Transition-Metal Reactions. *J. Phys. Chem. A* **2006**, *110*, 709−716.

(23) Steinmetz, M.; Grimme, S. Benchmark Study of the Performance of Density Functional Theory for Bond Activations with (Ni,Pd)-Based Transition-Metal Catalysts. *ChemistryOpen* **2013**, *2*, 115−124.

(24) Frisch, M. J.; Trucks, G. W.; Schlegel, H. B.; Scuseria, G. E.; Robb, M. A.; Cheeseman, J. R.; Scalmani, G.; Barone, V.; Petersson, G. A.; Nakatsuji, H.; Li, X.; Caricato, M.; Marenich, A. V.; Bloino, J.; Janesko, B. G.; Gomperts, R.; Mennucci, B.; Hratchian, H. P.; Ortiz, J. V.; Izmaylov, A. F.; Sonnenberg, J. L.; Williams-Young, D.; Ding, F.; Lipparini, F.; Egidi, F.; Goings, J.; Peng, B.; Petrone, A.; Henderson, T.; Ranasinghe, D.; Zakrzewski, V. G.; Gao, J.; Rega, N.; Zheng, G.; Liang, W.; Hada, M.; Ehara, M.; Toyota, K.; Fukuda, R.; Hasegawa, J.; Ishida, M.; Nakajima, T.; Honda, Y.; Kitao, O.; Nakai, H.; Vreven, T.; Throssell, K.; Montgomery, J. A., Jr.; Peralta, J. E.; Ogliaro, F.; Bearpark, M. J.; Heyd, J. J.; Brothers, E. N.; Kudin, K. N.; Staroverov, V. N.; Keith, T. A.; Kobayashi, R.; Normand, J.; Raghavachari, K.; Rendell, A. P.; Burant, J. C.; Iyengar, S. S.; Tomasi, J.; Cossi, M.; Millam, J. M.; Klene, M.; Adamo, C.; Cammi, R.; Ochterski, J. W.; Martin, R. L.; Morokuma, K.; Farkas, O.; Foresman, J. B.; Fox, D. J. *Gaussian 16*, Revision A.03; Gaussian, Inc.: Wallingford, CT, 2016.

DOI: 10.1021/acs.inorgchem.9b01630
Inorg. Chem. XXXX, XXX, XXX−XXX